www.elsevier.com/locate/memsci

Enhancing Water Vapor Permeability in Mixed Matrix Polypropylene Membranes Through Carbon Nanotubes Dispersion

G. Bounos, K.S. Andrikopoulos, H. Moschopoulou, G.Ch. Lainioti, David Roilo, Riccardo Checchetto, T. Ioannides, J.K. Kallitsis, G.A. Voyiatzis

PII: S0376-7388(16)32370-5
DOI: http://dx.doi.org/10.1016/j.memsci.2016.11.076
Reference: MEMSCI14916

To appear in: *Journal of Membrane Science*

Received date: 19 April 2016
Revised date: 24 October 2016
Accepted date: 26 November 2016

Cite this article as: G. Bounos, K.S. Andrikopoulos, H. Moschopoulou, G.Ch Lainioti, David Roilo, Riccardo Checchetto, T. Ioannides, J.K. Kallitsis and G.A Voyiatzis, Enhancing Water Vapor Permeability in Mixed Matrix Polypropylene Membranes Through Carbon Nanotubes Dispersion, *Journal of Membran Science,* http://dx.doi.org/10.1016/j.memsci.2016.11.076

Enhancing Water Vapor Permeability in Mixed Matrix Polypropylene Membranes Through Carbon Nanotubes Dispersion

G. Bounos[1], K.S. Andrikopoulos[1], H. Moschopoulou[1,3], G.Ch. Lainioti[1,2], David Roilo[4], Riccardo Checchetto[4], T. Ioannides[1*], J.K. Kallitsis[1,2], G.A. Voyiatzis[1*]

[1]*Institute of Chemical Engineering Sciences, Foundation for Research and Technology-Hellas, 26504 Patras, Greece*

[2]*Department of Chemistry, University of Patras*

[3]*Department of Chemical Engineering, University of Patras*

[4]*Department of Physics, University of Trento, via Sommarive 14, I-38123 Povo (TN), Italy.*

e-mail: theo@iceht.forth.gr

e-mail: gvog@iceht.forth.gr

***Corresponding authors.** Dr. T. Ioannides, FORTH/ICE-HT, Stadiou Str, Platani, GR-26504, Hellas, Tel:+302610965264.

***Corresponding authors:** Dr. G.A. Voyiatzis, FORTH/ICE-HT, Stadiou Str, Platani, GR-26504 Patras, Hellas, Tel:+302610965253 fax: +302610965223.

ABSTRACT

The water vapor and gas permeability of mixed matrix membranes (MMMs) composed by multiwalled carbon nanotubes (MWCNTs) dispersed in isotactic polypropylene (i-PP) was examined. The agglomeration state of the anisotropic filler nanoparticles was monitored by Raman spectroscopy and optical/electron microscopy in samples with different filler concentration and filler-matrix compatibility. The water vapor permeability of the MWCNT-MMM increases with the filler content up to a critical concentration. At larger MWCNT concentrations the composite membranes becomes water impermeable: filler aggregates or/and labyrinth-type networks form and act as traps for migrating water. Using

functionalized PP-chain grafted MWCNTs (MWCNT-g-PP) at 4 wt % critical concentration the water permeability increases by a factor ~ 35 compared to the pure i-PP membranes. The transport rate of light gases (N_2, H_2, CH_4 and CO_2) is not affected by the filler loading and dispersion. The selective enhancement of the water transport rates in the slightly altered i-PP matrix is attributed to the formation of regions consisting of well dispersed MWCNT interconnecting surrounding polymer layers with enhanced water permeability. The potential of such type of CNT-based polymer composite membranes is obvious for advanced filtration and separation applications.

Keywords: Mixed matrix polymeric membranes; Polypropylene carbon nanotubes composite membranes; Water vapor permeability; Gas selectivity; Gas seperation

1. Introduction

Carbon nanotubes (CNTs) exhibit interesting properties such as temperature stability, mechanical strength and chemical inertness which render them important additives of polymer nanocomposites [1,2]. Recently, CNTs have been also proposed as nanoporous fillers in Mixed Matrix Membranes (MMMs) for molecular separation [3,4]. The tubular structure of CNTs provides, in fact, structurally perfect and stable nano-channels with size at molecular dimensions. Tailoring channel size at the nanoscale level allows tuning of the interaction between diffusing molecules and CNT pore walls [5,6,7].

Procedures for manufacturing CNT-containing MMMs are easy to scale-up and attractive for their simplicity, time-sparing and inexpensive character, but the control and monitoring of CNT agglomeration in the polymer matrix still remains an open problem [2]. CNTs tend, in fact, to entangle with one another into bundles of rope-like crystalline structures that are strongly held together by Van der Waals forces due to their tube-like structure and high aspect ratio [8]. This agglomeration tendency increases by decreasing the number of graphitic layers of the nanotube, that is from multi-walled carbon nanotube (MWCNT) to single-walled carbon nanotube (SWCNT) due to the relevant increase in the nanotube surface curvature [9]. Covalent functionalization of the CNT sidewall is a versatile tool for enhancing the filler-matrix compatibility and thus filler dispersion due to the intermolecular interactions between polymer chains and functional groups grafted to CNTs [10].

Polypropylene (PP) is a semicrystalline thermoplastic polymer used in a variety of applications, including packaging and textiles. The compatibility of carbon nanofibers, organo-clays and CNT fillers with PP can be successfully improved by grafting with reactive moieties, such as acrylic acid, acrylic esters and maleic anhydride [11,12,13,14]. Recently Yang *et al.* prepared functionalized MWCNT through melt blending by using PP containing maleic anhydride and amine-functionalized MWCNTs: the PP- functionalized fillers (MWCNT-g-PP) dispersed well in the matrix leading to significant improvement in the mechanical performance of the composite [15]. MWCNT-g-PP can be also produced through a reaction of PP containing hydroxyl groups and MWCNTs bearing 2-bromoisobutyryl groups [16]. Radical mechanisms for attaching $(CH_2)_{10}CH_3$ alkyl chains (C_{11}) on MWCNTs sidewalls have also been reported [17] through thermal decomposition of lauroyl and dicumyl [18] peroxide.

The scientific literature reports several studies on fluid transport through CNTs, but experimental studies on the water transport properties of polymer CNT-MMM are scarce [3] and results are somewhat contradictory. Experimental investigation on CNT-PVA membranes indicates that the water transport rate increases with filler concentration as a consequence of the reduced crystallinity of the polymer matrix [19]. The opposite result was obtained in an experimental study on composites of multiwalled carbon nanotubes with segmented polyurethane (MWCNT-SPU) membranes where the decrease of water permeability with increase of filler content was attributed to the increased stiffness of the polymer chains [20]. In this

paper, we present a study on the water vapor transport through melt mixed isotactic polypropylene (i-PP) membranes containing MWCNTs of varying filler concentration and filler-matrix compatibility. The aim of this study is to examine the possible applications of these MMMs for advanced filtration/separation and to correlate their transport properties with the filler dispersion level. Filler compatibility was varied by PP chain grafting on MWCNT surface via melt blending of the copolymer PP-g-MA and the amino functionalized MWCNTs. The dispersion degree of MWCNTs fillers and the extent of filler agglomeration were monitored by Raman spectroscopy analyzing the CNTs vibrational modes, by the consideration of the composite crystallinity and through optical/electron microscopies. In order to obtain more detailed information on the mechanisms which control the transport of penetrant molecules, we have also measured the permeation of light gas molecules.

2. Experimental

2.1 Materials and membrane preparation methods

The isotactic polypropylene (i-PP) employed for film preparation was obtained from Ega-Chemie (Steinheim, Germany). Ethylenediamine and triethylamine were purchased from Sigma-Aldrich. The solvents, *N*,*N*-dimethylformamide (DMF), dry DMF, acetone and tetrahydrofuran (THF), were purchased from Fischer and used as received. Pristine MWCNTs (diameter 15-35 nm, length >10 μm code: NTX1) synthesized by chemical vapor deposition (CVD), as well as carboxylated MWCNTs (diameter 15-35 nm, length ~3-5 μm, code: NTX5) were kindly supplied by Nanothinx (Patras, Greece). Pristine MWCNTs, prior to melt-mixing, were sonicated for 10 min in ethanol and then dried in a hood at 60 ^{o}C for 48 hours. Their length after the sonication as confirmed by SEM was reduced to approximately 1.5 μm which is comparable to the respective length of the MWCNTs after their functionalization (see below).

For the synthesis of amino functionalized MWCNTs (MWCNT-NH_2), carboxylated MWCNTs (500 mg) were stirred in 40 mL thionyl chloride. The dispersion was placed in an ultrasonic bath for 30 minutes and then in an oil bath at 70 °C for 24 h. After the acyl chlorination, the solvent was removed in a rotary evaporator under nitrogen. The acyl-chlorinated nanotubes were reacted with 37.5 mL ethylenediamine and 1.25 mL triethylamine, using dry DMF as solvent, at 70 °C for 24 h. The amine functionalized CNTs

(MWCNTs-NH_2) were vacuum filtered through a Nylon membrane (200 nm) and washed several times with acetone, DMF and THF.

For the preparation of MWCNT-g-PP master batch, polypropylene grafted maleic anhydride (PP-g-MA, Sigma Aldrich, 427845) reacted with amine-functionalized MWCNTs toward direct grafting of polypropylene molecular chains onto the MWCNT surface. The reaction was performed in a homemade batch mixer at 200^{o}C for 30 minutes. Details for the preparation of the PP grafted MWCNTs have been reported elsewhere [15]. The efficiency of the MWCNT sidewall functionalization was confirmed by Attenuated Total Reflectance (ATR) vibrational spectra and thermogravimetric (TGA) analysis; TGA results are shown in Fig. 1. The content of MWCNT in MWCNT-g-PP master batch was estimated by TGA to be 30% wt.

Nanocomposite membranes containing either pristine or functionalized MWCNTs were prepared by melt mixing MWCNTs with appropriate amounts of i-PP in a homemade batch mixer at 185^{o}C for 15 min followed by melt pressing at 190 ^{o}C and 90 bars, 3 times for a few seconds each.

2.2 Experimental techniques

Optical microscope images were collected using an Olympus (Olympus Scientific Solutions, Massachusetts, USA) microscope (50x, NA=0.55) in the transmission mode. Differential scanning calorimetry (DSC) measurements were carried out on a Q100 unit (TA Instruments, New Castle, Delaware, USA) equipped with a controlled liquid N_2 cooling system. A cooling rate of 10 ^{o}C·min^{-1} and heating rates of ^{o}C·min^{-1} were used. The weight of the samples varied from 4 to 6 mg. In order to disregard the thermal history of the samples, the first cooling and second heating DSC runs were used for the analysis of the influence of MWCNT dispersion on the crystallization process. Crystallization degree as a function of MWCNTs loading thermographs were recorded upon the first heating (10 ^{o}C·min^{-1}).

Raman experiments were performed on an HR-800 JY UV-Vis-Raman system (Horiba Scientific, Jobin Yvon, Villeneuve d'Ascq, France), where excitation was performed by an air cooled He-Cd laser operating at 441.6 nm. The laser beam power measured on the sample varied from 0.02 μW to 11 mW. The backscattered configuration was selected using the 50x (NA=0.55) microscope objective. The scattered

beam was directed to the entrance slit of the single monochromators after passing through an appropriate edge filter. The spectral resolution was better than ~2.5 cm^{-1} for all measurements. The signal was recorded by a LN_2-cooled 2D-CCD detector. Instrument calibration was performed by regularly collecting the Neon lamp spectrum at the spectral windows of interest. Data analysis employed fitting with Lorentzian line profiles.

The "wet" cup method described by ASTM E 96-95 [21] was used to measure the water vapor transmission rate (WVTR) through the composite membranes. The WVTR is defined as the steady-state water vapor flow per time unit through a unit area of a body, occurring normal to its parallel surfaces, under specific controlled conditions of temperature and humidity at each of the two surfaces. According to this method, an acetal dish filled with distilled water and tightly covered by the examined membrane is placed in a homemade chamber at controlled conditions of 37 °C and 50% relative humidity (RH). The chamber consists of a homemade cartridge heater connected to a power supply and a temperature controller driven by an appropriate thermocouple, two inlets for N_2 (one for dry N_2 and one for humidified N_2) for humidity control via an internal humidity detector, a humidity controller and an axial fun for air circulation [22]. The effective membrane area was A=33.18 cm^2. The dish was removed and weighed every 2-3 hours in order to measure the mass of water lost as a function of time and calculate the WVTR in the steady-state region.

WVTR was calculated as follows:

$$WVTR = \frac{Mass\ H_2O\ lost}{time \times area} = \frac{flux}{area} \qquad (1)$$

with units of g d^{-1} m^{-2}. The *WVTR* value was normalized to the film thickness, *l*, in order to obtain the specific water vapor transmission rate, *Sp.WVTR= WVTR*l*, with units of g· d^{-1} ·m^{-2} μm. The *Sp.WVTR* is related to water vapor permeability, *P*, as:

$$P = \frac{Sp.WVTR}{\Delta P} = \frac{Sp.WVTR}{S(R_1 - R_2)} \qquad (2)$$

where *l* is the film thickness and Δ*P* is the water vapor partial pressure difference across the membrane, *S* is the saturation vapor pressure at test temperature, R_1 and R_2 the relative humidity inside the dish and chamber, respectively. Wet cup measurements were carried out at 37 ^oC under humidity conditions of

R_1=100 % and R_2=50 %. At 37 °C, the saturation water vapor pressure is 46 mmHg. A correction on this value to 36 mmHg [23] is performed because of the N_2 atmosphere.

Samples shaped in the form of discs with thickness between 80 and 200 μm were used for gas transport measurements by gas phase permeation technique. After fixing the (sample) temperature, one side of the membrane was exposed to the pure test gas kept at constant pressure P_{HPS} (HPS: High Pressure Side), while the other side (LPS: Low Pressure Side) faced a constant volume chamber evacuated by a turbomolecular pump. A valve permits sectioning of the pumping system from the constant volume chamber. Assuming as trigger time of the experiment ($t = 0$) the instant when the HPS of the membrane is exposed to the test gas (with the sectioning valve closed), the pressure increase in the constant volume chamber $P_{LPS}(t)$ is recorded by a spinning rotor gauge. P_{LPS} changes with time following the relation:

$$P_{LPS}(t) = \frac{RT_{cham}}{V_{cham}} AQ(t) \qquad (3)$$

where R is the universal gas constant, A the membrane area, while V_{cham} and T_{cham} are the volume and temperature of the constant volume chamber, respectively. $Q(t)$ is the amount of gas permeated per unit area of the membrane at time t. When the permeation process is controlled by the solution-diffusion mechanism, $Q(t)$ is given by the equation:

$$Q(t) = \frac{DSP_{HPS}}{l}\left[t - \frac{l^2}{6D}\right] \qquad (4)$$

where D and S are the gas diffusivity and solubility in the membrane material [24]. The intercept of the $P_{LPS}(t)$ signal on the time-axis defines the so-called time-lag, τ_L,

$$\tau_L = l^2/6D \qquad (5)$$

from which the gas diffusivity D can be calculated. The gas permeability can be evaluated by measuring the rate of pressure increase $\frac{dP_{LPS}(t)}{dt}$ in the constant volume chamber. CO_2, H_2 and N_2 with purity > 99.99 % were chosen as test gas; measurements were done at temperatures between 17 and 97 °C, with $P_{HPS} < 10^5$ Pa. Details on the experimental apparatus and procedures can be found in [25].

Gas permeation measurements were also carried out in a Wicke-Kallenbach set-up. The permeance of H_2O, CO_2 and CH_4 as single components was measured using He as sweep gas at 23 ^oC. All gaseous flows were adjusted using mass flow controllers (Aera FC-7700C). The feed and sweep flow rates were 50 cm^3 min^{-1}. The pressure on both sides, feed and permeate, was kept atmospheric. The gas composition at the permeate side was determined using a Shimadzu gas chromatograph (GC-2014) equipped with a thermal conductivity detector. The adsorption of water on MWCNT, pristine and functionalized, was examined in a laboratory setup for dynamic experiments interfaced to a quadrupole mass spectrometer for continuous on-line monitoring of cell exit gas. The carbon nanotube samples were exposed to a helium flow saturated with water vapor at room temperature for 15 min. The flow was then switched to pure helium and linear heating at 10 ^oC min^{-1} was commenced as soon as the m/z=18 signal was stabilized. No water desorption was observed during heating up to 150^oC.

3. Results and Discussion

3.1 Dispersion of MWCNTs in the composites

3.1.1 Morphology of the films

Optical microscopy

The MWCNT dispersion in the i-PP matrix appears to be strongly dependent on their functionalization as exemplified in the samples containing functionalized MWCNTs with the same nominal MWCNT loading (0.5 wt %). As illustrated in Fig.2, a decrease of the MWCNT agglomeration tendency is observed in the microscope transmission photographs of composites containing pristine MWCNTs and functionalized MWCNT-g-PP. The smallest average agglomerate size is evidently found in the composites containing MWCNT-g-PP.

Scanning Electron Microscopy

SEM images help to clarify the considerable difference in nanotube dispersion in i-PP/MWCNTs composites. In all examined composite membranes, both individual carbon nanotubes and agglomerates were found in the liquid nitrogen fractured cross sections as illustrated in Fig.3a and b. In the specific case of i-PP/MWCNT-g-PP, a very limited number of agglomerates were present. The observations in terms of

structural and morphological properties of the above mentioned composite membranes are in consistency with those reported in the literature [26,27].

Additionally, as illustrated in Fig.3c, by focusing inside within the formed agglomerates, the fractured surfaces reveal evident nanotube pull-out indicating low interfacial interaction between the PP matrix and MWCNTs in the composite containing pristine MWCNTs. According to the morphology of the fractured surfaces in Fig.3d, MWCNT chemical functionalization provides compatibilization between the modified nanotubes and the polymer matrix, since nanotube pull-out becomes not prominent; this behavior shows higher adhesion between the polymer and MWCNT-g-PP in comparison with pristine MWCNTs.

3.2 Raman spectra of powders and nanocomposites

Fig.4 shows the Raman spectrum of pristine MWCNT in the form of powder, the spectrum of MWCNT-g-PP in the form of master batch as well as the spectra of their corresponding i-PP nanocomposites both of 0.5% wt. nominal loading. Earlier works involving multiwall carbon nanotubes indicate four dominant features in their Raman spectra; namely the G band at ~1580 cm^{-1}, the D band at ~1360 cm^{-1}, the second-order G' band at ~2700 cm^{-1} and the D' band at ~1620 cm^{-1}. The G band is a doubly degenerate phonon mode (E_{2g} symmetry) that is Raman active for sp^2 carbon networks while the D and D' bands are defect-induced Raman features [28]. In general, the less disordered the graphite-based systems are, the weaker the intensities of the D, D' bands (in the respective Raman spectra) are expected to be. Thus, in a single Raman spectrum, the ratio of the intensity of the D band (I_D) to the respective intensity of the G band (I_G) has been frequently used as an indicator of the disorder of the graphitic based system. I_D/I_G is ≈ 0.78 for the case of pristine MWCNTs signifying their good quality. Besides, the ratio appears to be somewhat increased to ≈ 0.81 for the MWCNT-g-PP master batch at the same laser power, indicating that during the functionalization and the melt mixing process some minor additional disorder is created on the graphitic-based samples, which has been used as an argument for the successful functionalization [29]. It should be noted that the I_D/I_G ratio of the composite films cannot be calculated reliably due to the strong interference of the i-PP bands with the MWCNTs' D band.

The MWCNT powder and MWCNT-g-PP master batch appear to be rather homogeneous, i.e. the spectral band shapes remain roughly unchanged for all spectra obtained from different spots on the sample. Nevertheless, close inspection of band positions indicated slight alterations depending on the focal field

scanned on the sample at each measurement. The spectra depicted in Fig.4 are actually averaged spectra obtained from measurements performed on eight different spots of each sample. Essentially, the G band appears at 1577±2.3 cm^{-1} for the pristine MWCNTs and at 1584±1.3 cm^{-1} for the MWCNT-g-PP master batch. Indicative of the presence of grafted PP species are the characteristic C-H stretching bands around 2900 cm^{-1} in the spectrum of MWCNT-g-PP. In both spectra, the relative intensity of D´ shoulder ($I_{D'}/I_G$) does not change. Similarly the D´ band intensity maximum is up-shifted by grafting PP macromolecules in MWCNT-g-PP masterbatch. Analogous behavior is also observed for D-band and G´-band peak position frequency which are up shifted from 1353 cm^{-1} (pristine MWCNT) to 1357 cm^{-1} (MWCNT-g-PP) and from 2702 cm^{-1} to 2707 cm^{-1}, respectively.

Contrary to the optical homogeneity of the powder and the master batch, most of the composite films are considerably inhomogeneous; this can be spectroscopically revealed by just inspecting the intensity of the peaks attributed to i-PP in comparison to the respective intensity of peaks attributed to the MWCNTs. The spectra from the films in Fig.4, which are normalized with respect to the i-PP band intensity, indicate that the intensity of the nanotubes' G band differs for each sample despite the fact that all samples possess the same MWCNT loading. Furthermore, in spite of the inhomogeneity of the composite films, the position of the G band appeared to be the same for each of the eight different measurements undertaken for the three different samples studied; moreover, the respective calculated statistical error appeared to be significantly smaller and the position of the G band notably higher than the one of the powders i.e. 1585.5±1.2 cm^{-1}. The positions of G, D and G' bands are marked with dashed lines in Fig.4 and the G position of all examined systems is also presented in Fig.5 for two extremely different cases of excitation power along with the associated calculated error bars. The vibrational contribution of PP appeared in all the composite spectra; the Raman bands at 1375 and 1455 cm^{-1} are assigned to the bending vibration of CH_3, whereas the corresponding band at ~2900 cm^{-1} represents the stretching vibration of CH. PP bands were not shifted to higher frequencies with regard to those of the unfilled polymer. Similar observations were reported in MWCNT/rubber composite studies [30], as a consequence of the physical constraints introduced to the polymer chains by the presence of nanotubes. The absence of double bonds in the case of polypropylene could reduce the electronic interactions between polymer and nanotubes resulting in absence of changes in the polymer bands. Importantly and in contrast to PP bands, the G band of incorporated MWCNTs was

shifted to a higher frequency by 8 cm^{-1} compared with the pristine MWCNT powder, while a shift of 7 cm^{-1} is observed in the case of MWCNT-g-PP master batch and i-PP/MWCNT-g-PP film. Given the same MWCNT loading of the composites, as well as the same excitation power, the slight difference on the observable shift may express the differences in the extent of MWCNT agglomeration because of the compatibility with i-PP matrix, as it was confirmed by optical and scanning electron microscopy. The difference in the extent of MWCNT agglomeration induces a local perturbation of MWCNT concentration which is sensitively monitored by G-Band shifting, as reported previously [31]. This observation is a clear proof for the potential of Raman spectroscopy to probe the MWCNT dispersion state inside a polymer matrix.

For testing the hypothesis of how MWCNT dispersion can be precisely evaluated by Raman spectroscopy, Raman spectra were selectively obtained over a region with well dispersed MWCNT and a region with MWCNT agglomerates inside the i-PP\MWCNT composite using the self-contained microscope, operating under confocal configuration. The results are illustrated in Fig.5. Error bars in the G-band position are determined by averaged spectra obtained from measurements performed on eight different spots of each sample. It is worth mentioning that the G-band position recorded from the focusing volume with well dispersed MWCNTs is upshifted by about 6 cm^{-1} as compared with the corresponding peak position from agglomerates. Furthermore the observation of the G-band of the agglomerates being very close to the one of pristine MWCNT powder underlines the significance of the fact that the G-band shift originates from the increase of absorptivity due to the close packing of the MWCNTs in the agglomerates, and not from the functionalization process. In other words, the close packing of MWCNTs results in an increase of temperature when probed by the laser beam which affects the G-band position [32,33].

Light grey columns in Fig.5 illustrate the variations in G-band for a very low excitation power of 0.02 mW. The position of the G-band was found to be the same for all the examined systems. According to earlier studies on the laser heating of MWCNTs [32,33], the effect on G-band position can be explained on the basis of elongation of C-C bonds due to thermal expansion. The similar G-band position for all examined samples at very low power indicates that the main contribution on Raman vibrations stems from a temperature effect and not from the exerted pressure from the polymer to MWCNT.

3.3 Crystallization kinetics

Differential Scanning Calorimetry (DSC) thermographs of neat i-PP and i-PP composites are shown in Fig. 6 and the resulting thermodynamic properties are summarized in Table 1. The degree of crystallinity of i-PP composites is calculated from the melting thermographs (1st heating, heating rate = 10 ^{o}C min^{-1}) by the following equation: $X_c = \frac{\Delta H_m}{(1-\varphi)\Delta H_0}$, where ΔH_m is the heat of fusion of the measured sample, ΔH_0 is the heat of fusion for 100% crystalline i-PP and φ is the weight fraction of CNT in the nanocomposites. ΔH_0 was taken equal to 209 J g^{-1} [34]. The degree of crystallinity, X_c, appears to decrease with incorporation of MWCNT in the i-PP matrix, for the same nominal loading of 0.5% wt., whereas the crystallization onset temperature, T_{oc}, and peak crystallization temperature, T_c, shift to higher values in the presence of MWCNTs. Additionally, the crystallization peak is narrower in the case of nanocomposites. The i-PP/MWCNT composite exhibits the least significant change in T_{oc} and T_c compared to the neat i-PP, which is attributed to the low loading and poor dispersion. The significant shift in T_{oc} and T_c observed for the i-PP/MWCNT-g-PP composite is attributed to the increased number and uniform dispersion of active nucleation sites compared to the poorly dispersed MWCNTs in i-PP/MWCNT sample. These findings are consistent with previous results on the crystallization behavior of PP/CNT composites [35,36,37] and confirm that the functionalized MWCNTs are better dispersed than pristine MWCNTs, and that the dispersion is maintained with increasing nanotube concentration up to the critical loading, i.e. 2 % wt for membranes containing pristine MWCNT and 4% wt for membranes containing MWCNT-g-PP. Similar trends were observed in melting behavior (second heating is used to avoid the inconsistencies of the non-systematic ice quenching during film preparation).

In the case of pure i-PP, the two main melting peaks are located at 158.2 and 162.4 ^{o}C. The peak at high temperatures is attributed to the melting of *a*-crystals, whereas the broad peak at the temperature range 150–160 ^{o}C corresponds to melting of *b*-crystals, or smaller/imperfect *a*-crystals [38]. The former does not apply here, since X-ray diffraction patterns do not show any presence of *b*-crystals (results not shown). The melting peaks are narrower in the nanocomposites; this suggests a narrower crystallite size distribution as compared to the i-PP matrix. The melting temperature, T_m, of the composite containing functionalized

MWCNTs is also slightly lower than the one of the composite containing pristine MWCNT. Additionally, the presence of the broad peak at 155 ^{o}C is an indication of formation of smaller crystals. The higher thermal conductivity of CNTs, as compared to that of the polymer, allows heat to be more evenly distributed in the nanocomposites, and explains, at least in part, the sharper crystallization and melting peaks [37].

Fig. 7 shows the dependence of X_c as a function of MWCNT loading. Insignificant changes are observed in X_c as the amount of MWCNT increases up to a critical loading, i.e. 2 wt.% in the case of MWCNT and 4 wt.% in the case of MWCNT-g-PP, respectively. Similar trends have been reported in the literature for iPP/MWCNT composites [35,37]. The degree of crystallinity is reduced remarkably at loadings higher than critical loadings.

3.4 Water vapor and gas transport

The water vapor permeability values of composite films were measured by the wet cup method at 37 ^{o}C. The permeability value of i-PP films was 460 Barrer, in accordance with values reported in the literature [39]. The ($P/P_{i\text{-}PP}$) ratio of permeability of nanocomposites to the permeability of pure PP is presented in Fig. 8 as function of filler concentration. It can be observed that the water vapor permeability of i-PP/MWCNT membranes increases up to a critical filler concentration of 2 wt % where $P/P_{i\text{-}PP}$ attains its maximum value, ~22: the permeability decreases strongly for higher filler concentrations. A similar behavior is also observed for i-PP/MWCNT-g-PP membranes but the maximum $P/P_{i\text{-}PP}$ ratio is slightly higher and appears at a higher filler concentration (4 wt %), showing that the permeability value is related to the appearance of agglomerates. In order to confirm this result, the water vapor permeability along with CH_4 and CO_2 permeability of i-PP and i-PP/MWCNT-g-PP membranes was also measured with a Wicke-Kallenbach diffusion cell coupled to a gas chromatograph using as test samples a pure i-PP membrane and an i-PP/MWCNT-g-PP membrane with 4 wt % filler concentration. Results are reported in Table 2.

Measurements indicate that the water vapor permeability of the membrane strongly increases after the addition of the MWCNT-g-PP filler confirming the findings of the wet cup method. Table 2 also shows that addition of the MWCNT-g-PP filler does not influence the CH_4 and CO_2 permeability. Hence, the H_2O/CO_2

selectivity which is ~ 9 for the i-PP membrane, in good accordance with the literature [40], increases to ~ 122 for the membrane containing MWCNT-g-PP filler.

Additional permeation measurements were carried out as a function of temperature using H_2, N_2 and CO_2 as a test gas and i-PP/MWCNT-g-PP membranes with filler concentration ranging from 0.25 to 6 wt %. The measured values of gas diffusivity D and gas permeability Φ are presented in Figs. 9a and 9b: reported data are average values (statistical errors are smaller than the size of symbols). It is worth mentioning that: i) N_2 permeability and diffusivity values are not presented at temperatures lower than 60° C due to the low signal-to-noise ratio of the measurements and ii) the H_2 diffusivity was too high to obtain reliable measurements with the employed time-lag method. The activation energy values for permeation, E_Φ, and diffusion, E_D, of the three test molecules, as evaluated from the Arrhenius plot of experimental data in Figs. 9a and 9b, are reported in Figs. 10a and 10b, respectively [41,42]. Note that the E_Φ and E_D values of the nanocomposite membranes appear independent of the filler content and are equivalent to the values obtained with the pure i-PP membrane. Results in Figs. 9 and 10 indicate that the MWCNT addition does not change the gas permeation properties of i-PP membranes, see Table 2, and that the diffusion mechanism of the penetrant molecules in composite membranes is the same as in the i-PP matrix.

The results of vapor and gas transport analysis can be summarized as follows: i) MWCNT-g-PP addition up to a critical loading increases the water vapor permeability of the i-PP membrane, ii) for loadings larger than the critical one the composite membrane becomes almost impermeable to water vapor and iii) MWCNT-g-PP addition does not change the gas permeation properties of the membranes.

In MMMs, molecular transport is controlled by the solution-diffusion mechanism. Because in the present samples the filler addition does not change the crystallinity degree of the matrix, see Fig.7, then the filler dispersion can influence the transport properties by: i) affecting the polymer chain packing thus inducing changes of the polymer free volume and ii) producing defects such as pores and nano-voids at the polymer-filler interface [8]. The fractional free volume in polymers is defined as $f_h = V_f / V$ where V is the macroscopic specific volume of the matrix and V_f is the specific free volume: $V_f = V - V_O$, with V_O being the specific volume occupied by the polymer chains [43].The free volume theory of diffusion provides the following relation between the diffusivity D of penetrant molecules in the polymer layers and the polymer

fractional free volume: $D = A_d \exp (-B_d / f_h(T))$, where A_d is a parameter specific of the polymer-penetrant system, while B_d depends on the size of the penetrant molecules [44]. Interphase pores act as fast diffusion channels because here the transport of penetrant molecules follows Knudsen diffusion: $D_K = (d_p/3)(8\,RT / \pi\, m)^{1/2}\, (1-\sigma_{mol}/2d_p)$: here, d_p is the pore diameter, while m and σ_{mol} are the mass and size of the penetrant molecule, respectively [45]. The previous relations clearly indicate that, both, the variations of the fractional free volume and the formation of interphase pores are expected to influence the transport rates of all penetrant molecules in a similar manner. Therefore, it can be safely concluded that these mechanisms cannot account for the selective increase of water transport rates in the present MMMs samples.

We, thus, suggest that the transport properties of the present nanocomposite samples are in relation with specific properties of the filler-H_2O penetrant system. Porous fillers, as the present open-ended MWCNTs, dispersed in the polymer matrix may change the transport rate of penetrant molecules depending on the size of pore and/or on the adsorptive characteristics of the pore surface [8]. In this experiment, penetrant molecules have similar size (kinetic diameter) and the selective increase of the H_2O transport rates is thus in relation to the H_2O selective "repulsion" capability.

The results of the present experiments can be explained describing the MMM as a two-phase system consisting of a polymer matrix and a second pseudo-dispersed phase exhibiting enhanced water vapor permeability [46]. This pseudo-dispersed phase consists of high aspect ratio MWCNT with the surrounding matrix interphase region. Taking into account that no measurable water desorption was found on the specific CNT samples employed in the present work, the enhanced water permeability of the composite membranes can be attributed mainly to enhanced water diffusivity. This phenomenon could be due to the atomic-scale smoothness of CNT walls facilitating molecular ordering and establishing an almost friction-less transport mechanism of water [46,47,48,49].

When filler particles are well dispersed, an increase of their concentration gives rise to an increase of the water vapor permeability because a progressively larger volume fraction of the membrane is occupied by this pseudo-dispersed phase. This picture is compatible with the finding that the $P/P_{i\text{-}PP}$ ratio is larger for MMMs with CNTs: in fact the functionalized filler exhibits higher matrix compatibility and thus dispersion degree. Moreover: i) the presence of non-reacted COOH and NH_2 groups (originating from the MWCNT-g-

PP synthesis route) on the functionalized filler sidewall effectively increase the hydrophilic character of the filler-matrix interphase layers.

At filler concentrations larger than the critical values, the water permeation rate decreases and membranes become almost impermeable. This blockage effect can be attributed neither to an increase of the crystallinity degree of the matrix nor to an increased stiffness of the polymer chains, but is correlated with the formation of filler agglomerates or/and a labyrinth-type network formation. The exact underlying mechanism, however, is hard to explain at this stage.

Conclusions

The dispersion of functionalized MWCNTs selectively enhances the water vapor permeability of i-PP membranes and has no effect on the permeability of light gases, such as H_2, N_2, CH_4 and CO_2. Structural analysis of composites bearing different filler content and filler compatibility with the polymer matrix shows that the water vapor permeability enhancement is related to the high degree of filler dispersion. The best performances in terms of water vapour transmission rates are obtained using functionalized CNT at a filler loading of 4 wt. %. The improved H_2O permeability is consequence of the formation of dispersed CNT regions in the matrix with fast transport rates for water formed by the MWCNT filler and the grafted polymer layers. Given the simplicity of the preparation method, the results point out the potential of the CNT-based melt pressed polymer composite membranes for advanced filtration and separation applications.

Acknowledgements

The present work was funded by Synergasia 2009 program (project code: 09SYN-1156) and KRIPIS PROENYL program (project code: ΣΠΑ00190-3). The programs are co-funded by the European Regional Development Fund and national resources. DA and RC thank Provincia Autonoma di Trento (Italy) for the ENAM project (No. 220068/s116).

LIST OF TABLES

Table 1: *Xc is the degree of crystallinity calculated from enthalpy of melting of second melt, ΔH_m Enthalpy of melting, ΔH_C Enthalpy of crystallization, Melting temperature (T_m), onset of crystallization temperature (T_{oc}) and crystallization temperature (T_c) for the pure i-PP matrix and i-PP/MWCNT nanocomposites. It is noted that the effective MWCNT loading is 0.5% wt.*

	T_{oc} (°C)	T_c (°C)	T_m (°C)	ΔH_m	X_c (%)
	Crystallization		*2nd Melting*		
i-PP	118.2	123.7	162.7	93.0	44.5
i-PP/MWCNT	122.8	125.7	163.3	88.9	42.7
i-PP/MWCNT-g-PP	124.6	127.2	161.3	85.8	41.3

Table 2: *Gas permeability of i-PP and i-PP/MWCNT-g-PP membranes. Measurement at 23 °C with a Wicke-Kallenbach cell.*

		Permeability (Barrer)		
Membrane	**Thickness (μm)**	**H_2O vapor**	**CH_4**	**CO_2**
Pure i-PP	70	18.40	0.06	1.95
i-PP/MWCNT-g-PP (4 wt.%)	110	254	0.07	2.08

FIGURE LIST

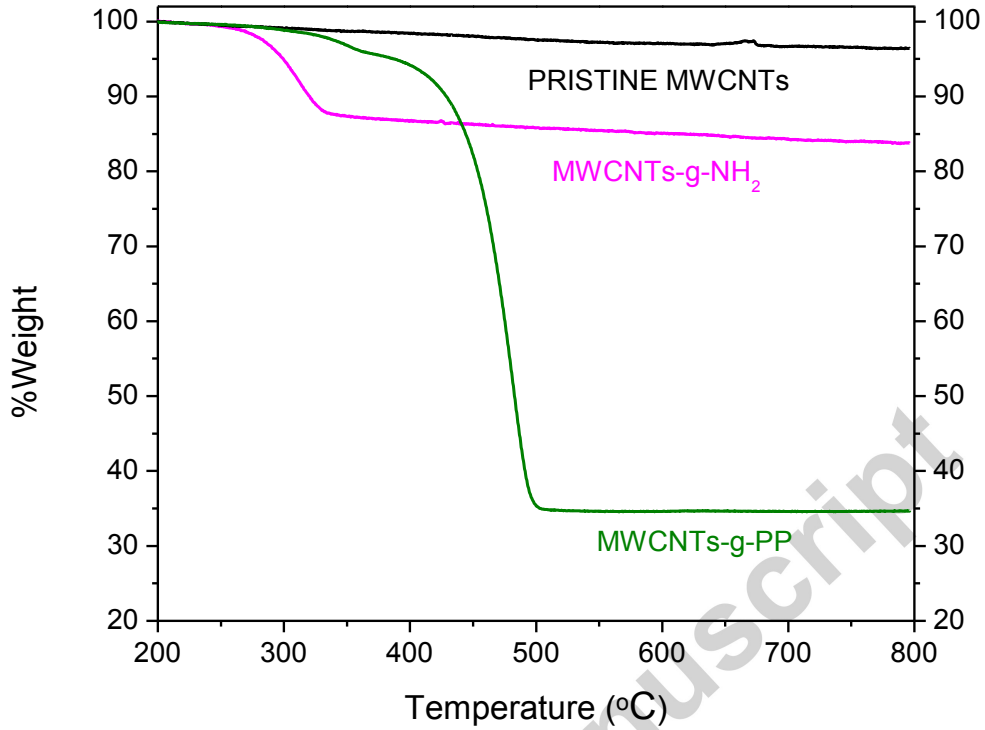

Figure 1

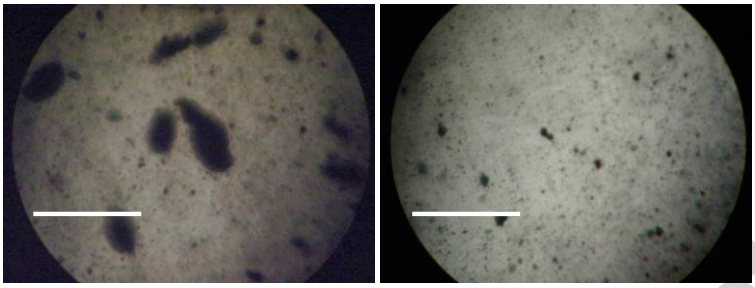

Figure 2

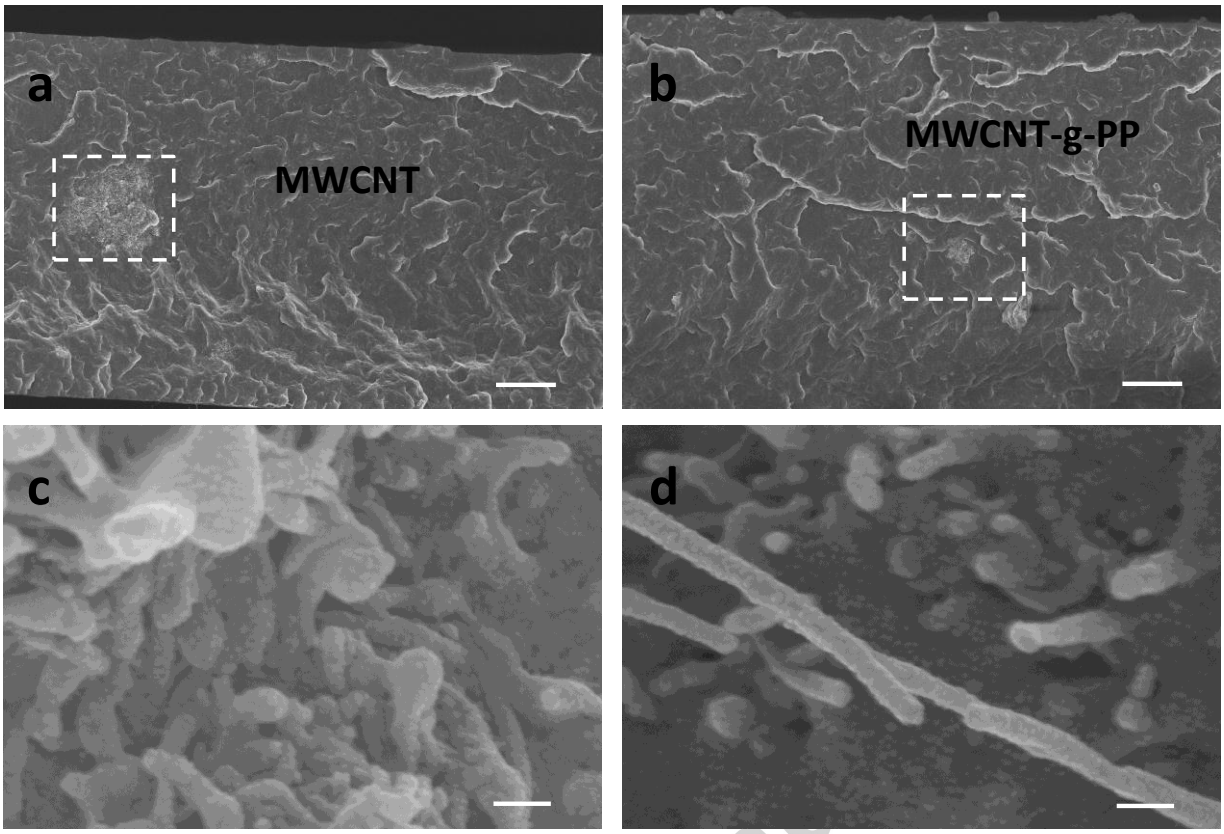

Figure 3

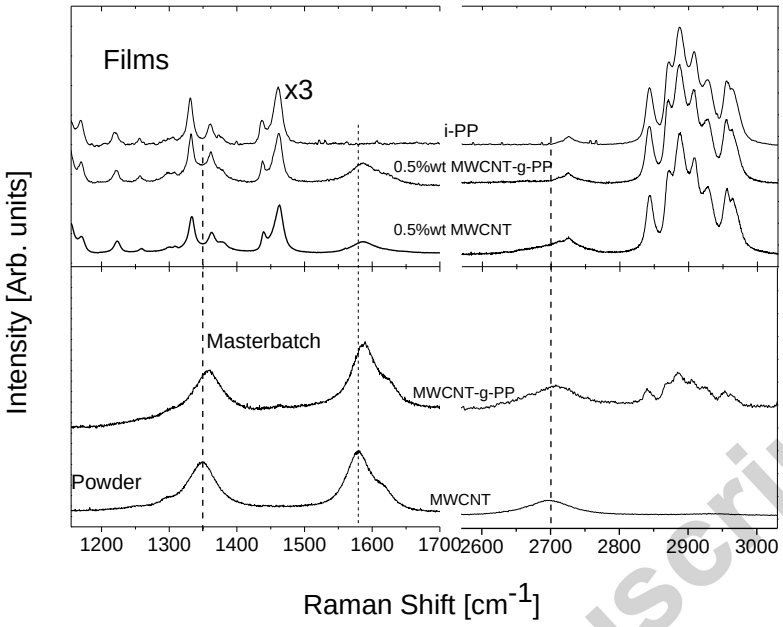

Figure 4

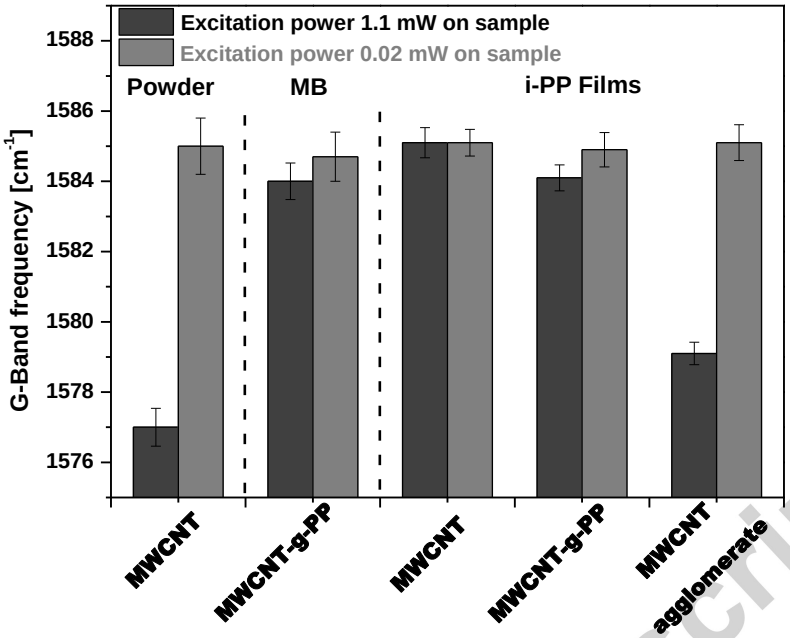

Figure 5

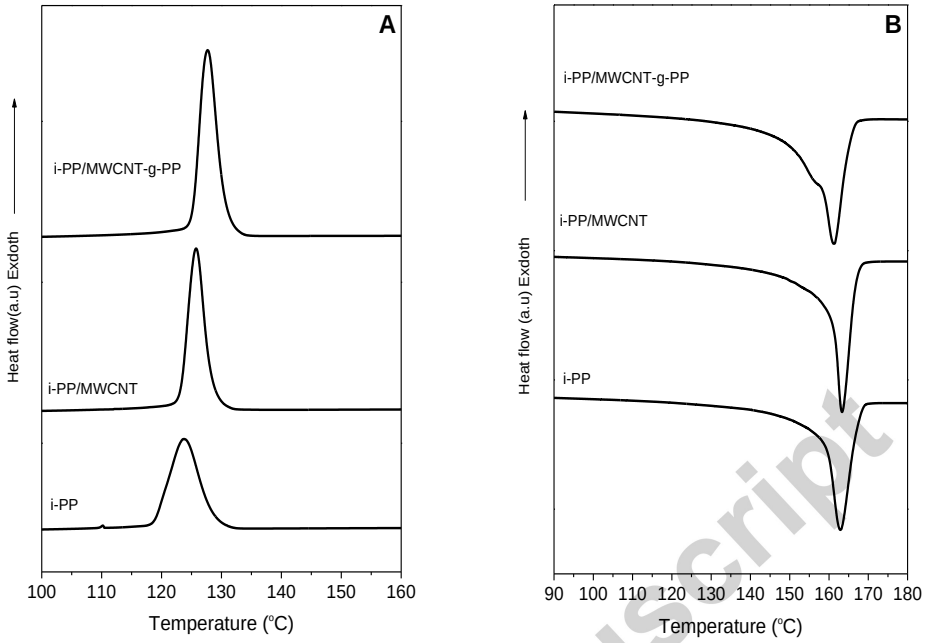

Figure 6

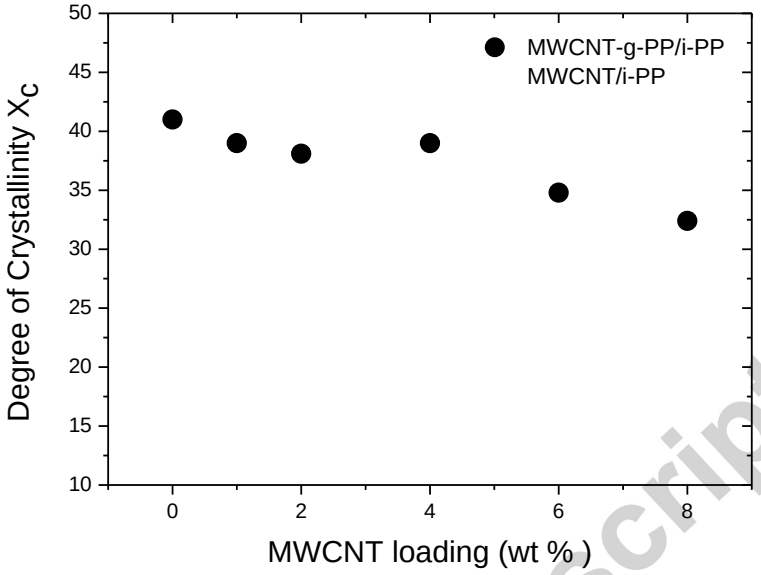

Figure 7

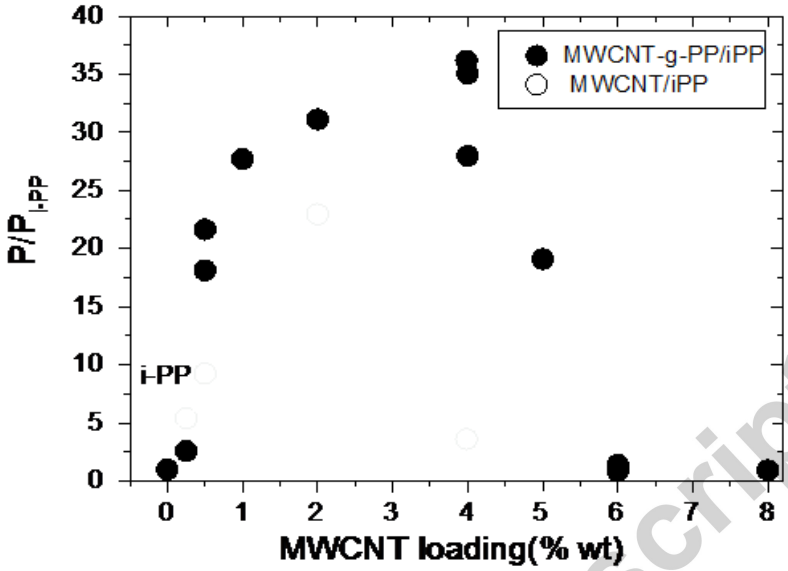

Figure 8

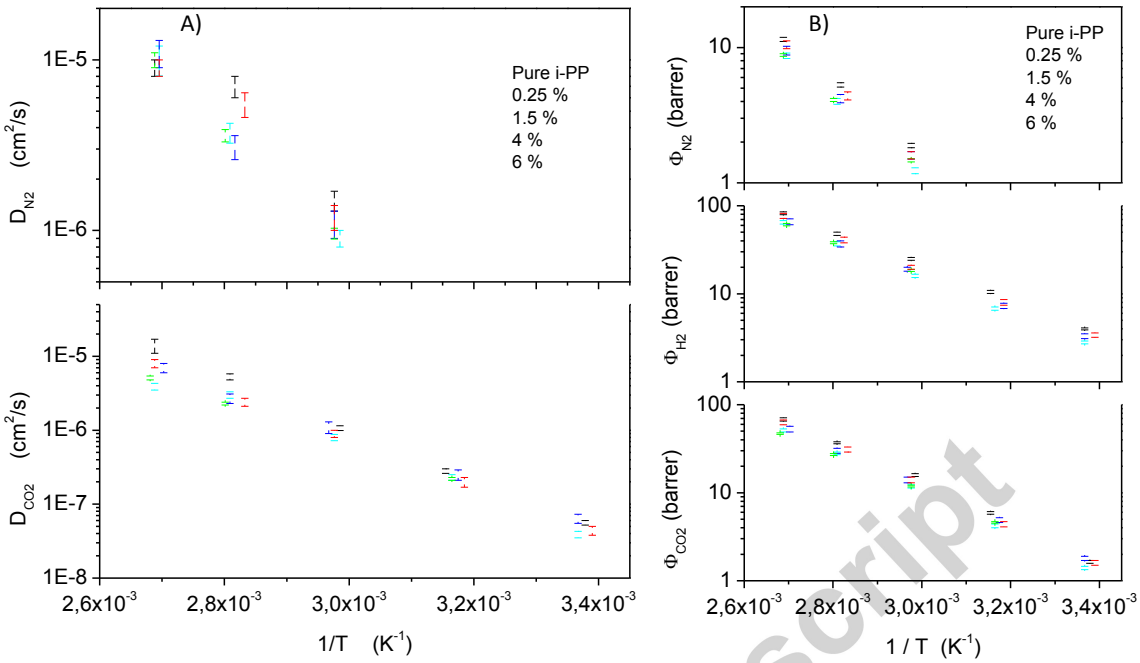

Figure 9

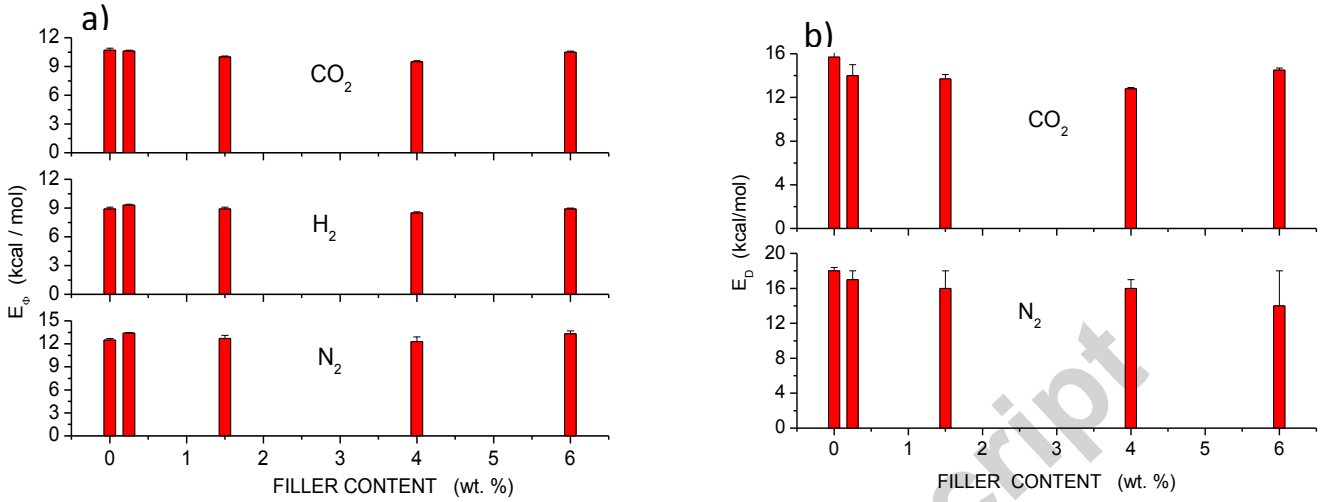

Figure 10

FIGURE CAPTIONS

Figure 1: Weight loss as a function of temperature for pristine MWCNTs, MWCNTs-g-NH_2, MWCNTs-g-PP masterbatch and the copolymer PP-g-MA. TGA performed under N_2 atmosphere, at 10^oC/min.

Figure 2: Transmission mode optical micrographs of the i-PP composites containing the same loading, 0.5 wt % of a) MWCNT, b) MWCNT-g-P.

Figure 3: SEM images of liquid nitrogen fractured cross sections of composite membranes with MWCNT loading of 0.5 wt %. Photos a and b were recorded from i-PP/MWCNT and i-PP/MWCNT-g-PP cross sections respectively, with a spatial resolution of 20 μm. MWCNT agglomerations are indicated by white arrows. Photos c and d shows the area within the agglomeration with spatial resolution 100 nm indicated by white dashed squares in photos a and b respectively.

Figure 4: Raman spectra of MWCNT powder (spectra depicted are the average spectra of eight different spots on each sample), MWCNT-g-PP master batch and their composite films (individual spectrum for each sample). All spectra were recorded using 0.5 mW laser power on the samples.

Figure 5: Representation of G-band position of all MWCNT samples: powder, MWCNT-g-PP master batch (MB) and the respective i-PP composite films (0.5 wt % MWCNT loading). The dark grey columns represent the G-band position in the spectra recorded with excitation power 1.1 mW and the light grey columns with excitation power 0.02 mw respectively.

Figure 6: A) Crystallization thermographs for pure i-PP and nanocomposites (heating rate: 10 $^oC \cdot min^{-1}$). B) Melting thermographs for pure i-PP and nanocomposites (heating rate: 5 $^oC \cdot min^{-1}$ $^oC \cdot min^{-1}$).

Figure 7: Degree of crystallinity of i-PP composites as a function of MWCNT loading.

Figure 8: Water vapor permeability enhancement ratio $P/P_{i\text{-}PP}$ as a function of filler concentration for i-PP/MWCNT-g-PP and i-PP/MWCNT membranes.

Figure 9: CO_2 and N_2 diffusivity (A) and permeability (B) of i-PP and i-PP/MWCNTg-PP membranes.

Figure 10: The activation energy values for permeation E_Φ (A) and diffusion E_D (B) of the three test molecules.

REFERENCES

[1] G.S. Nanada, R. Sravendra, W.C. Jae, L. Lin, and H.C. Siew, Polymer nanocomposites based on functionalized carbon nanotubes, Prog. Polym. Sci. 35 (2010) 837-867.

[2] J. N. Colòeman, U. Khan, W. J. Blau and Y. K. Gun'ko, Small but strong: A review of the mechanical properties of carbon nanotube–polymer composites, Carbon 44 (2006) 1624-1652.

[3] A. F. Ismail, P. S. Goh, S. M. Sanip and M. Aziz, Transport and separation properties of carbon nanotube-mixed matrix membrane, Sep. Purif. Technol. 70 (2009) 12-26.

[4] G. Dong, H. Li and V. Chen,Challenges and opportunities for mixed-matrix membranes for gas separation, J. Mater. Chem. A 1 (2013) 4610-4630.

[5] M. Whitby and N. Quirke, Fluid flow in carbon nanotubes and nanopipes , Nature Nanotechnol. 2 (2007) 87-94.

[6] S. Konduri, H. M. Tong, S. Chempath, S. Nair, Water in Single-Walled Aluminosilicate Nanotubes: Diffusion and Adsorption Properties, J. Phys. Chem. C 112 (2008) 15367-15374.

[7] S. Jakobtorweiher, M. G. Verbeek, C. P. Lowe, F. J. Keil, B. Smith, Understanding the Loading Dependence of Self-Diffusion in Carbon Nanotubes, Phys. Rev. Lett. 95 (2005) 044501-4.

[8] V. Georgakilas, A. Bourlinos, D. Gournis, T. Tsoufis, C. Trapalis, A. Mateo-Alonso, M. Prato, Multipurpose organically modified carbon nanotubes: from functionalization to nanotube composites, J. Am. Chem. Soc. 130 (2008) 8733-8740.

[9] X. Liu, M. Wang, S. Zhang and B. Pan, Application potential of carbon nanotubes in water treatment: A review, J. Envirn. Sci. 25 (2013) 1263-1280.

[10] S.M. Sanip, A.F. Ismail, P.S. Goh, T. Soga, M. Tanemura and H. Yasuhiko, Separation Properties of Functionalized Carbon Nanotubes Mixed Matrix Membranes, Sep. Purif. Technol. 78 (2011) 208-213.

[11] A. Kelarakis, K. Yoon, I. Sics, R.H. Somani, X. Chen, B.S. Hsiao, et al. Shear-induced orientation and structure development in isotactic polypropylene melt containing modified carbon nanofibers, J. Macromol. Sci. Phys. 45 (2006) 247-261.

[12] N. Ristolainen, U. Vainio, S. Pavola, M. Torkkeli, R. Serimaa, J. Seppälä, Polypropylene/organoclay nanocomposites compatibilized with hydroxyl-functional polypropylenes, J.Polym.Sci.Polym.Phys. 43 (2005) 1892-1903.

[13] X. Zhou, X. Xie, F. Zeng, RK-Y. Li, Y-W. Mai, Properties of polypropylene/carbon nanotube composites compatibilized by maleic anhydride grafted SEBS,Key. Eng. Mater. 312 (2006) 223-228.

[14] C.A. Mitchell, J.L. Bahr, S. Arepalli, J.M. Tour, R. Krishnamoorti, Dispersion of functionalized carbon nanotubes in polystyrene. Macromolecules 35 (2002) 8825–8830; C.A. Dyke, J.M. Tour, Separation of Single-Walled Carbon Nanotubes on Silica Gel. Materials Morphology and Raman Excitation Wavelength Affect Data Interpretation, J Phys Chem A 108 (2004) 11151–11159 ; R. Blake, Y. K. Gun'ko, J. Coleman, M. Cadek, A. Fonseca, J.B. Nagy, W. Blau, A generic organometallic approach toward ultra-strong carbon nanotube polymer composites. J. Am. Chem. Soc. 126 (2004) 10226–10227; D. Tasis, N. Tagmatarchis, A. Bianco, M. Prato. Chemistry of carbon nanotubes, Chem Rev 106 (2006) 1105–1136

[15] B-X. Yang, J-H. Shi, K.P. Pramoda, S.H. Goh, Enhancement of the mechanical properties of polypropylene using polypropylene-grafted multiwalled carbon nanotubes, Comp. Sci. Tech. 68 (2008) 2490-2497 ; B-X. Yang, K.P. Pramoda, G.Q. Xu, and S. H. Goh Adv. Funct. Mater. Mechanical Reinforcement of Polyethylene Using Polyethylene-Grafted Multiwalled Carbon Nanotubes, 17 (2007) 2062-20699.

[16] Jeon J-H, Lee S-H, Lim J-H, Kim K-M, Fabrication and Characterization of Homogeneous Composites of Polypropylene and Multiwalled Carbon Nanotubes, J. Appl. Polym. Sci. 124 (2012) 3064-3073.

[17]A.A. Koval'chuk, V.G. Shevchenko, A.N. Shchegolikhin, P.M. Nedorezova, A.N. Klyamkina, A.M. Aladyshev, Effect of carbon nanotube functionalization on the structural and mechanical properties of polypropylene/MWCNT composites, Macromolecules 41 (2008) 7536-7542.

[18] G. Farzi, S. Akbar, E. Beyou, P. Cassagnau, F. Melis, Effect of radical grafting of tetramethylpentadecane and polypropylene on carbon nanotubes' dispersibility in various solvents and polypropylene matrix, Polymer 50 (2009) 5901-5908.

[19] J. H. Choi, J. Legal, W. N. Kim, Modification of performances of Various Membranes Using MWCNTs as a Modifier, Macromol. Symp. 249-250 (2007) 610-617.

[20] S. Mondal, J.L. Hu, Microstructure and Water Vapor Transport Properties of Functionalized Carbon Nanotube-Reinforced Dense Segmented Polyurethane Composite Membranes, Polym. Eng. Sci. Volume 48 (2008) 1718-1724.

[21] Standard test methods for water vapor transmission of materials, ASTM E96/E96M-10, DOI:10.11520/E0096_E0096M-10

[22] K. S. Andrikopoulos, G. Bounos, D. Tasis, L. Sygellou, V. Drakopoulos and G. A. Voyiatzis, The Effect of Thermal Reduction on the Water Vapor Permeation in Graphene Oxide Membranes, Adv. Mater. Interfaces,1 (2014) 1400250 (1-8)

[23] J A. Dean, Lange's Handbook of Chemistry, 14th edition, McGraw-Hill, Inc

[24] J. Crank, "The Mathematics of Diffusion" (Oxford University Press, Oxford, 1975).

[25] R. Checchetto, A. Miotello, L. Nicolais and G. Carotenuto, Gas transport through nanocomposite membrane composed by polyethylene with dispersed graphite nanoplatelets, J. Membr. Sci. 463 (2014) 196-204

[26] S.H. Lee, E. Cho, S.H. Jeon, J.R. Youn, Rheological and electrical properties of polypropylene composites containing functionalized multi-walled carbon nanotubes and compatibilizers, Carbon 45 (2007) 2810-2822.

[27] K. Prashantha, J. Soulestin, M.F. Lacrampe, M. Claes, G. Dupin, P. Krawczak, Multi-walled carbon nanotube filled polypropylene nanocomposites based on master batch route: Improvement of dispersion and mechanical properties through PP-g-MA addition, Express Polym. Lett. 2 (2008) 735-745.

[28] M.A. Pimenta, G. Dresselhaus, M.S. Dresselhaus, L.G. Cançado, A. Jorio, R. Saito, Studying disorder in graphite-based systems by Raman spectroscopy, Chem Phys Chem Phys 9 (2007) 1276-1290.

[29] Y. Zhang, A. A. Broekhuis, M.C.A. Stuart, T.F. Landaluce, D. Fausti, P. Rudolf, and F. Picchioni, Cross-Linking of Multiwalled Carbon Nanotubes with Polymeric Amines, Macromolecules 41 (2008) 6141-6146.

[30] L. Bokboza, J. Zhang. Raman spectroscopic characterization of multiwall carbon nanotubes and of composites, Express Polym. Lett. 6 (2012) 601-608.

[31] G. Bounos, K.S. Andrikopoulos, T.K. Karachalios, G.A. Voyiatzis, Evaluation of multi-walled carbon nanotube concentrations in polymer nanocomposites by Raman spectroscopy, Carbon 76 (2014) 301-309.

[32] E. Fitzer, F. Rozploch, Laser Raman spectroscopy for determination of the C-C bonding length in carbon, Carbon 26 (1998) 594-595.

[33] P.V. Huong, R. Cavagna, P.M. Anaya, O. Stephan, Temperature-dependent vibrational spectra of carbon nanotubes, Phys Rev B 51 (1995) 10048-10051.

[34] J. Brandrup, Immergut, E.A. Grulke, A. Abe, D.R. Bloch. Polymer handbook. John Wiley & Sons; 1999.

[35] L. Valentini, J. Biagiotti, J.M. Kenny, S. Stucki, Effects of single-walled carbon nanotubes on the crystallization behavior of polypropylene, J Appl Polym Sci 87 (2003) 708–713.

[36] M. Ganß, B.K. Satapathy, M. Thunga, R. Weidisch, P. Pötschke, A. Janke, Temperature dependence of creep behavior of PP–MWNT nanocomposites, Macromol. Rapid Commun. 28 (2007) 1624–1633.

[37] E. Logakis, E. Pollatos, Ch. Pandis, V. Peoglos, I. Zuburtikudis, C.G. Delides, A. Vatalis, M. Gjoka, E. Syskakis, K. Viras, P. Pissis, Structure–property relationships in isotactic polypropylene/multi-walled carbon nanotubes nanocomposites, Comp.Sci.Techn. 70 (2010) 328–335.

[38] A.R. Bhattacharyya, T.V. Sreekumar, T. Liou, S. Kumar, L.M Ericson, R.H. Huge, et al. Crystallization and orientation studies in polypropylene/single wall carbon nanotube composite, Polymer 44 (2003) 2373–2377.

[39]J. A. Barrie, in "Diffusion in Polymers" J. Crank and G. S. Park Eds. Academic Press, 1968.

[40] S. Zeman, L. Kubik, Permeability of polymeric packaging materials, Techn Sc, 10 (2007) 26-34

[41] A. Fernández-Barquín, C. Casado-Coterillo, M. Palomino, S. Valencia, A. Irabien, LTA/poly(1-trimethylsilyl-1-propyne) mixed matrix membranes for high-temperature CO_2/N_2 separation. Chem. Eng. Technol. 38 (2015) 658-666.

[42] E. Santos, E. Rodríguez-Fernández, C Casado-Coterillo, A. Irabien, Hybrid ionic liquid-chitosan membranes for CO2 separation: Mechanical and thermal behavior. Int. J. Chem. React. Eng. 13 (2015) 1-6.

[43] W. M. Lee, Selection of barrier materials from molecular structure, Polym. Eng. Sci. 20 (1980) 65-69.

[44] H. Lin and B. D. Freeman, Gas Permeation and Diffusion in Cross-Linked Poly(ethylene glycol diacrylate), Macromolecules 39 (2006) 3568-3580; P. N. Patil, D. Roilo, R. S. Brusa, A. Miotello, S. Aghion, R. Ferragut and R. Checchetto, Free volumes and gas transport in polymers: amine-modified epoxy resins as a case study. Phys. Chem. Chem. Phys. 18 (2016) 3817-3824.

[45] R. E. Cunningham and R. J. J. Williams, Diffusion in Gases and Porous Media (Plenum Press, New York, 1980).

[46] M.A. Aroon, A. F. Ismail, T. Matsuura and M. M. Montazer-Rahmati, Performance studies of mixed matrix membranes for gas separation: A review, Sep. Purif. Technol. 75 (2010) 229-242.

[47] A. Kalka, S. Garde and G. Hummer, Osmotic Water Transport through carbon nanotubes membranes, PNAS 100 (2003) 10175-10180.

[48] I. Yzeiri, N. Patra and P. Kràl, Porous carbon nanotubes: Molecular adsorption, transport and separation, J. Chem. Phys. 140 (2014) 104704-5.

[49] Z. Mao and S. B. Sinnot, A computational study of molecular diffusion and dynamic flow through carbon nanotubes, J. Phys. Chem. B 104 (2000) 4618-4624.

Highlights

- **The MWCNT dispersion within the *i*PP matrix was extensively characterized utilizing a variety of techniques.**
- **Water vapor permeability enhancement is observed with the incorporation of MWCNTs.**
- **The water vapor permeability enhancement is related to the degree of MWCNT dispersion.**
- **The MWCNT incorporation into the *i*PP matrix has no effect on the permeability of light gases.**